Binary Optical True-Time Delay Based on the White Cell: Design and Demonstration

Betty Lise Anderson, *Senior Member, IEEE*, David J. Rabb, Carolyn M. Warnky, and Feras Abou-Galala, *Student Member, IEEE*

***Abstract*—An optical true-time delay device that uses a binary counting system in a modified White cell is demonstrated. The switching engine uses four spherical mirrors and a three-state digital micromirror array. The delay part, as designed, provides 6 bits of delay ranging from 78 ps to 5 ns, using a combination of dielectric blocks for short delays and lens trains for longer ones. Long lens trains are folded for compactness. The authors describe the design and demonstrate two of the 6 bits of delays experimentally. Delays were accurate to within the measurement resolution of 1.25 ps. The insertion loss varied from 3.1–5.2 dB, depending on delay. It was found that the micromirrors do not contribute significantly to the loss.**

***Index Terms*—Array signal processing, beam steering, microelectromechanical devices, optical delay lines, optical signal processing, phased array radars.**

I. Introduction

THE WHITE CELL has been adapted for massively parallel optical true-time delay (OTTD) devices for steering of very large phased array antennas [1]–[6]. The original White cell, invented in the 1940s for spectroscopy [7], allows a light beam to circulate among three spherical mirrors for a fixed number of round trips. The beam is focused to a spot once per round trip; at other places, it is allowed to diverge. Although spectroscopists generally require only a single light beam, many beams can in fact circulate among the same set of mirrors; each beam generates a unique spot pattern, which is a property that we exploit. The general idea is that several White cells share a microelectromechanical-system (MEMS) micromirror array, which switches light beams among various White cells, some of which introduce time delays. A key feature of this approach is that it uses free space (as opposed to waveguides). Since light beams can overlap in space without interfering, the OTTD can be made very compact even when the number of light beams is very large. The White-cell approach can provide an arbitrary number of different delays for thousands of antenna elements, limited only by the number of pixels on the MEMS.

The MEMS itself is digital, meaning it has a fixed number of discrete tip angles, as opposed to analog MEMS that can tip to any angle but require feedback systems to maintain angle accuracy. The White cell is, by its very nature, insensitive to MEMS mirror pointing errors [8]; due to the discrete nature of the MEMS, the controlling electronics is simple.

White-cell-based OTTDs come in two basic types. The first is the polynomial White cell [1], [2], [4], in which the number of delays N is proportional to some polynomial in m, where m is the number of bounces a given light beam makes, e.g., a quadratic cell makes $N \propto m^2$ delays. The second class is the exponential White cell, in which the number of delays is proportional to some number raised to the power of the number of bounces; e.g., a binary cell has $N \propto 2^m$. Since the exponential number grows faster than a polynomial, the exponential cells are the preferred choice when large numbers of delays are needed. This paper discusses the first demonstration of a binary-White-cell OTTD device.

II. Binary White Cell

A. Switching Engine

The binary White cell has two main parts, a switching engine and a delay section. The switching engine is shown in Fig. 1. A three-state MEMS tilting mirror array is at the left. The mirrors can tip to one of the three angles: -10°, 0° (flat), and $+10^\circ$. At the right are four spherical objective mirrors that we call White-cell mirrors. There are also four field lenses. An auxiliary mirror and a delay plane are on either side of the MEMS. The delay plane is not a physical device; it is a plane that is conjugate to the MEMS and acts as the entrance to the delay section. For now, we will treat it as a plane mirror. There are also two points labeled "centers of curvature (CCs)," which are the intersections of the axes of the four White-cell mirrors with the MEMS/auxiliary mirror/delay plane (we will call it the MEMS plane from now on). Actually, these points are the images of the physical CCs, through the appropriate field lens, that appears on this plane. We will explain the significance of the CCs next.

To understand how a binary cell works, it is necessary to know how the spot pattern develops for a particular light beam. A light beam enters the White cell via an input turning mirror, which is a small fixed mirror here, in the plane of the auxiliary mirror, that sends an input beam to the White-cell mirror labeled "A" in Fig. 1. The input beam is conditioned to focus to a spot on the input turning mirror, and it diverges on its way to A. White-cell mirror A sees this input spot as an object and produces an image (another spot) of an equal and opposite distance around A's CC (CCA), as shown in Fig. 2. Since CCA is located between the auxiliary mirror and the MEMS, the image lands on the MEMS. We have chosen one of the ten

Manuscript received July 18, 2005; revised September 29, 2005. This work was supported by the Defense Advanced Research Projects Agency.

The authors are with ElectroScience Laboratory, The Ohio State University, Columbus, OH 43212 USA (e-mail: anderson@ece.osu.edu; rabb.9@osu.edu; warnky.1@osu.edu; abou-galala.1@osu.edu).

Digital Object Identifier 10.1109/JLT.2006.871032

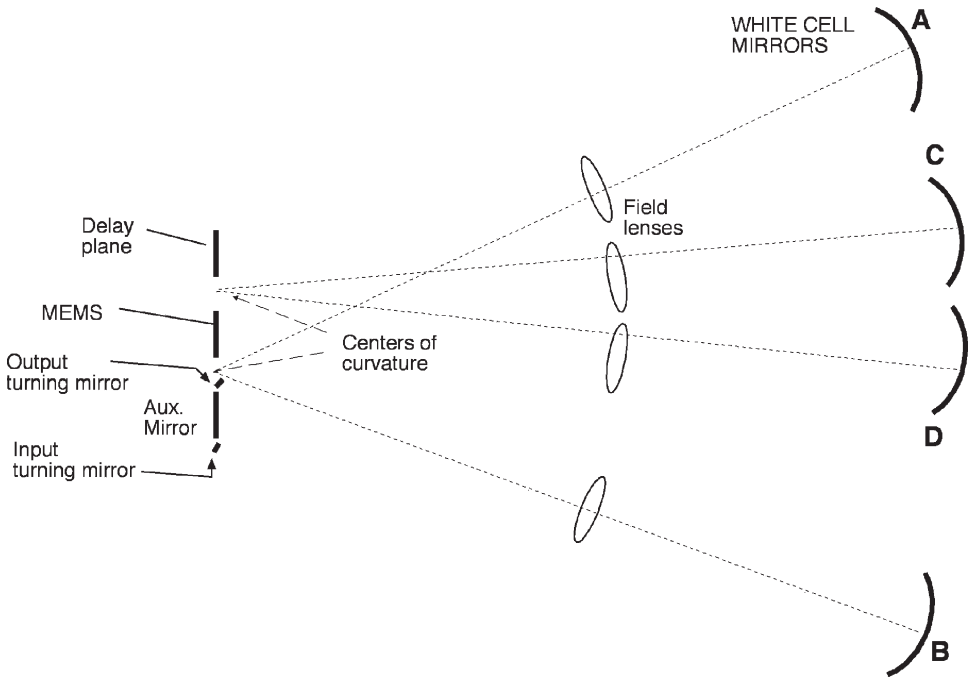

Fig. 1. Switching engine of a binary White cell.

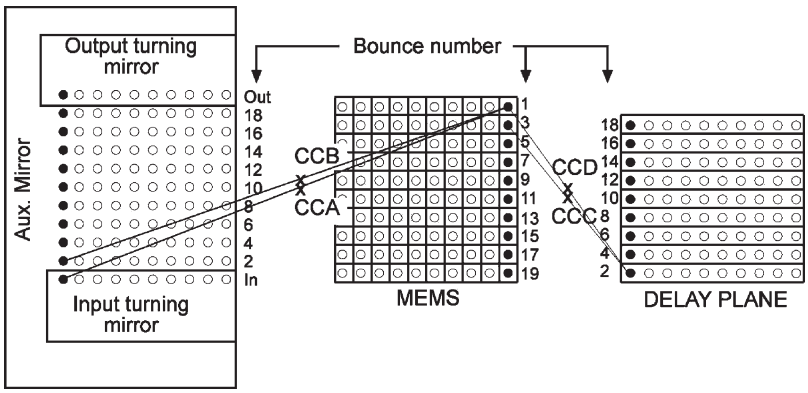

Fig. 2. Spot pattern in a White cell. Ten beams are inputs to the input turning mirror. The array of input beams is reimaged onto the top row of the MEMS. There, each mirror in the row can direct its light beam to either the auxiliary mirror or the delay plane on bounce 2.

input beams to follow (solid circles). Its first bounce lands in the top row of the MEMS, as shown. If the MEMS pixel is flat (set to 0°), the beam coming from A now goes to mirror B, forming a second spot image on the auxiliary mirror this time. If all the MEMS pixels in this column remain flat, the beam bounces back and forth between A and B and eventually lands on the output turning mirror, which sends it out of the cell into whatever output optics there are. Since the beam in this case never goes to the delay section, this represents the shortest time in which a beam can emerge from the White cell; all other paths will be longer. Thus, we reference all delays to the all-AB path and call the AB White cell the null cell.

On the other hand, if that first MEMS pixel were tipped to $+10^\circ$ (upward in Fig. 1), then the light coming from A would be sent next to D. The CC of mirror D is located between the MEMS and the delay plane; thus, in this case, the second spot image forms on the bottom row of the delay plane (which we are again treating as a simple mirror for the moment). The light reflects from the delay plane, going to mirror C, which images the second bounce back onto the MEMS, this time in the second row (labeled bounce 3). At this point, the MEMS can either send the beam back to the delay plane (pixel flat) or return it to the null cell (pixel at -10°). This can happen on every bounce on the MEMS. On the last bounce, the MEMS is programmed so that every beam lands on the output turning mirror.

B. Delay Section

Thus, the beam can be sent to the delay plane any number of times. We now introduce the delays. We let each row of the delay plane be associated with a different delay, and we let each delay be twice as long as that of the row below it. There are nine rows in the delay plane; thus, any delay from 0 to 2^9 can be selected for each beam independently.

Let us suppose that there is a glass block in the bottom row of the delay plane (see Fig. 3) and that the back of the block is reflective. The glass has some thickness, and the combination of the extra path and the higher refractive index causes the beam

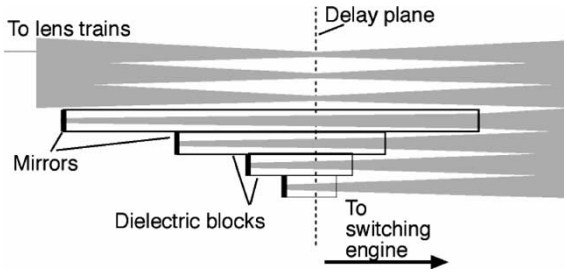

Fig. 3. Side view of dielectric blocks used as delays.

to take longer to go through the glass and emerge back into the switching engine. A block that is twice as long is in the next row. The fronts of the blocks do not lie on the delay plane but at different distances in front of it, depending on the delay chosen [5]. This is because the White cell has certain imaging conditions that must also be fulfilled for it to operate.

From the figure, it will be seen that there is a limit to how long a delay block can be, which will depend on the width of the delay-plane rows. If the block gets too long, the beam will be truncated. The rows are images of the MEMS-pixel rows, so the width depends on the pixel pitch. We have shown a single row of input spots, so each row is one spot or pixel-pitch high. If the inputs are in a two-dimensional array, then the delay-plane rows will be as tall as the input array. For example, if the inputs are in a 10×100 spot array, then the delay-plane rows can be 10 times the pixel pitch in height. However, a limit will still be reached eventually.

For long delays, we use lens trains. The details have been described before in [5]. However, briefly, a set of lenses is used to reimage a row of the delay plane to a mirror somewhere behind the delay plane. Fig. 4(a) shows a lens train with three lenses per group. The delay plane is at the right. A spot on the bottom row of the delay plane is reimaged by a lens labeled "imaging lens" to a flat mirror. The beam is delayed by going the extra distance and back. The light returns to the switching engine exactly as if it had been reflected from a mirror, but it has been delayed. The other two lenses between the delay plane and the flat mirror are field lenses.

A beam sent to the next row of the delay plane has to be delayed by twice as much. It can pass through the same lenses as the previous row, but the light can be made to miss the mirror and pass through to another mirror farther on. The idea here is that that the beams resolve into separate spots (where they can be individually manipulated) only at the MEMS and images of the MEMS, such as the delay plane or strip mirrors at various locations in the lens trains. Everywhere else, they overlap to some extent, overlapping completely at the White-cell mirrors. The side view shows the progress of three individual beams in the lens train. The top view shows that each beam arrives from one White-cell mirror (C), passes through the lens train on one side of the lens, and returns through the other side. After passing through the lens train and back through the delay plane, the light goes to mirror D. Note that the imaging lens in the center of each stage of the lens train is actually conjugate to the two White-cell mirrors C and D, which is a feature that we will exploit when we fold the lens train to make it more compact.

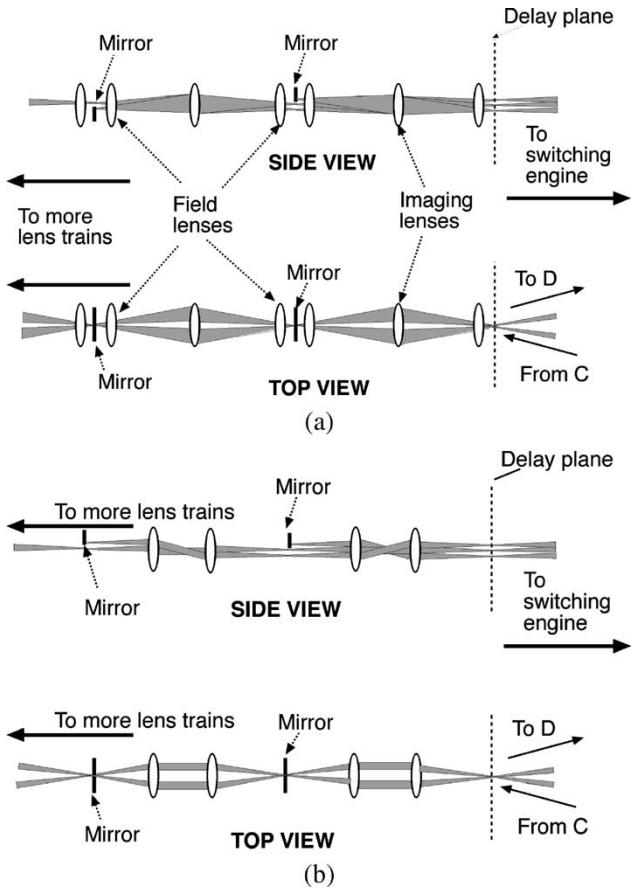

Fig. 4. Two ways to implement longer delays using a lens train. (a) Three lenses per stage. (b) Two lenses per stage.

However, before going on, we mention that there is another way to implement a lens train, as shown in Fig. 4(b). Here, there are only two lenses per group. The light is collimated between the two lenses. The operation is the same as the three-lens/group case, except that the image of the White-cell mirrors appears between the lenses in this case.

Then, suppose a time delay of several nanoseconds is required. This translates to a long skinny lens train, which is awkward from a packaging point of view. It is better to fold the lens train using imaging mirrors rather than lenses. If a beam is supposed to get a very long delay that includes passing through many stages of the lens train, the folded version of the lens train begins to look like another White cell, as we will see in Section III.

III. Design

We next present a specific binary-White-cell design. The specifications are that it should produce 6 bits of delay with a delay increment $\Delta = 78.125$ ps and a maximum delay of 5 ns. It will use an MEMS device (made by Sandia National Laboratories) that has a 10×10 array of square 100-μm pixels on a 250-μm pitch. Each pixel can tip to $\pm 10^\circ$ or 0°.

The mirrors are electrostatically actuated and employ stops for repeatable angle positioning within $\pm 0.05^\circ$. Measured mirror switching times with simple control signals are ~ 40 μs, and faster operation is possible. Prototype mirror arrays were

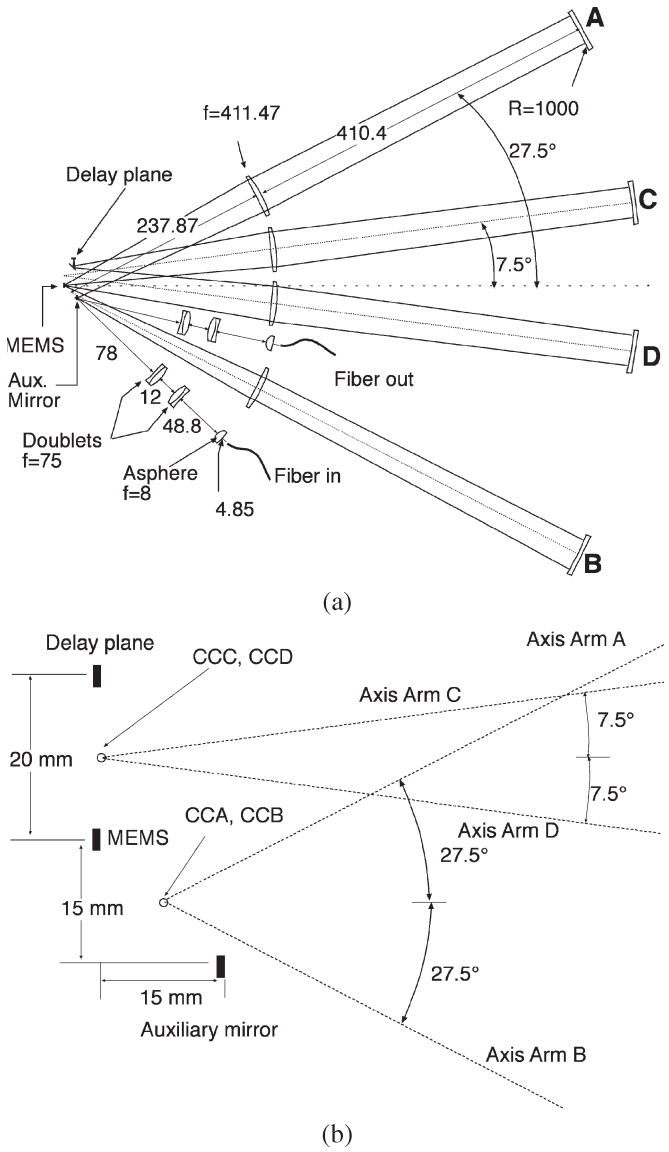

Fig. 5. Switching engine design. (a) Switching engine arms, including folding of path to delay plane. (b) Close-up of MEMS area. Folding omitted to simplify figure.

supplied with a controller board that provides a PC interface and generates all mirror control signals. In an initial life test of one mirror array, no mirror failed after $> 1\,000\,000\,000$ switching cycles in a laboratory environment.

A. Switching Engine

Fig. 5 shows the particulars of the switching engine. The auxiliary mirror is actually placed 15 mm in front of the MEMS plane, so that the mirror and its mount do not interfere physically with the MEMS package and the circuit board. The focal lengths, distances, and angles are shown with distances in millimeters and angles in degrees. The field lenses are plano-convex ($R = 206.0$ mm, thickness is 6.3 mm, with the convex side toward the White-cell mirrors). The diameters are 2 in and made of BK7 glass. The White-cell mirrors are also of 2-in diameters. In Fig. 5(b), a close-up of the MEMS region is shown

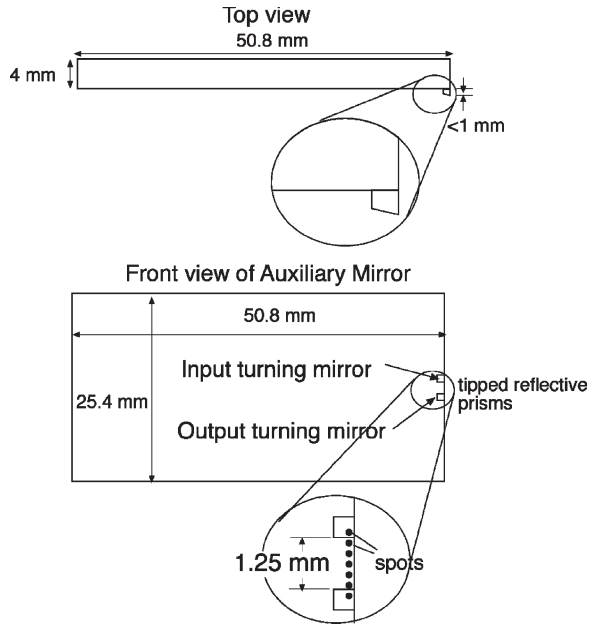

Fig. 6. Auxiliary mirror with input and output turning mirrors.

(with the folding omitted to simplify the figure). The images of the CCs are shown.

The input and output optics are located on axes as shown in the figure. The input is from a single mode fiber (mode field diameter ≈ 10 μm) with a wavelength of 1.55 μm. The input optics are designed to image the fiber onto the input turning mirror with a magnification of about 5. A 25-μm spot is optimal in the White cell, because it is small enough not to be truncated significantly by the MEMS pixels (100 μm on a side) but is as large as possible to minimize the beam divergence and thus avoiding vignetting by the field lenses and White-cell mirrors. We used a single input spot; to use multiple input spots (the eventual goal), microlens arrays will doubtlessly be needed since the spots must be magnified but the pixel pitch currently matches the pitch in commercial fiber arrays (250 μm). Similarly, the output optics demagnify the spot from the output turning mirror and image it onto the output fiber.

The input and output turning mirrors are fabricated by gluing microprisms to the auxiliary mirror; see Fig. 6. For a 6-bit system such as ours, there will be six spots on the auxiliary mirror, seven spots on the MEMS, one input spot, and one output spot. The spot spacing on the auxiliary mirror matches the pitch of the MEMS pixels, which dictates the placement of the input and output turning mirrors.

B. Delays

Then, we discuss the delays. We design the shortest four delays in silicon blocks of optical grade. The longest two delays (1.25 and 2.5 ns) are implemented as lens trains. For the experiment, our intent is to demonstrate only four of the six delay elements: the two shortest and the two longest.

The spot pattern is shown in Fig. 7. Light enters from the input turning mirror, goes to White-cell mirror B, and makes the first bounce on the MEMS. The pixel can be tipped to send

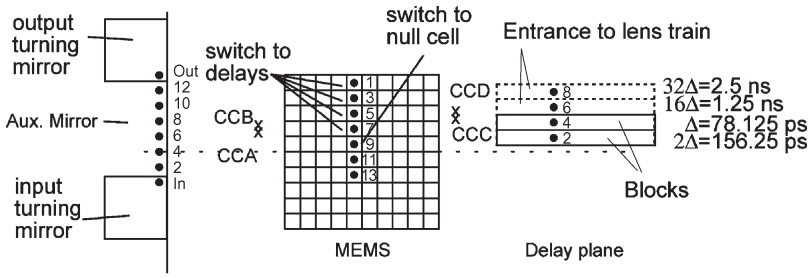

Fig. 7. Spot pattern in the apparatus.

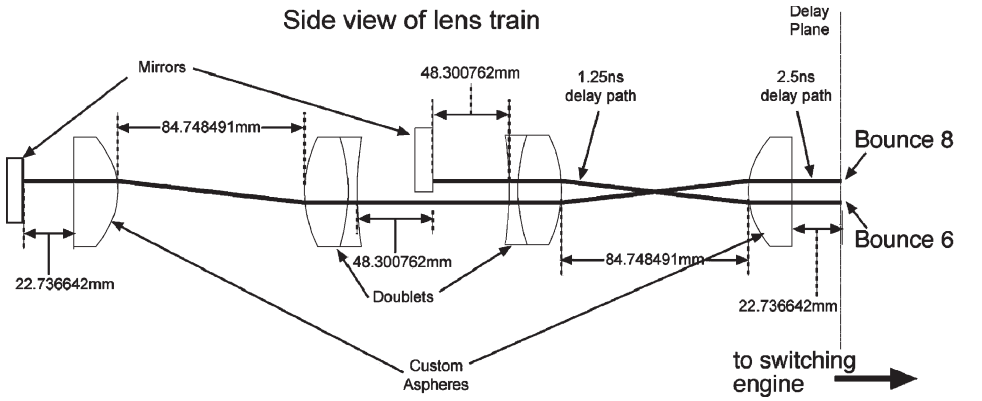

Fig. 8. Side view of unfolded lens train.

the light either to the auxiliary mirror (null path) or to the delay plane for bounce 2. In the row corresponding to bounce 2, there will be of a dielectric block that produces a delay of 156.25 ps. Similarly bounces 4, 6, and 8 can be sent to either the null or the delay path. For the two longest delays, we use a lens train.

1) Lens Train: We use the two-lens/group system shown earlier in Fig. 4(b). Fig. 8 shows the design. Light crossing the delay plane in the row of bounce 6 is reimaged to a spot on the first mirror, whereupon it returns and exits the delay plane in the same spot at which it entered. Looking from the top (not shown), the angle of entrance is equal and opposite to the angle of exit, that is, the light is coming from White-cell mirror C and returns to White-cell mirror D. Optically, the light behaves as if it had hit a plane mirror in the delay plane; in fact, it has traveled a longer path (longer by 1.25 ns). On bounce 8, the light sent to the delay plane will miss the first mirror and will be returned by the farther one, for a delay of 2.5 ns.

The aspheres are plano-convex with a 10-mm thickness and a 25.4-mm diameter. The radius of curvature of the curved surface is 14.44 mm, with fourth- and sixth-order deformation coefficients of 2.355×10^{-5} and 1.0182×10^{-7}, respectively. The doublet's first surface has a curvature of 23.88 mm and a thickness of 8.3 mm (in LAKN22); the second surface radius is -28.12 mm. The second material is SFL6 with a center thickness 1.8 mm and the final surface curvature is 112.08 mm.

The overall length of the lens train is about 350 mm, but it can be folded to make it more compact. We use another White cell to do this, as shown in Fig. 9. Here, we see the delay plane at the right. This is a side view, and we see the four rows of the delay plane of which the top two are the "windows" through which light passes to enter the lens train. Directly above these is a segmented mirror, of which the purpose we will discuss next; below it, are the delay blocks for the shorter delays.

In Fig. 9, the beam enters from the right, passes by the silicon blocks (discussed in the next section), goes through the field lens, and heads toward a spherical mirror labeled C′&D′ (because it is conjugate to both mirrors C and D in the delay cell of the switching engine). Here, we use a single mirror because, while C and D have different CCs in the switching engine, the CCs are coincident in the lens train so the same mirror can be used. If the light is sent to the delay cell on the sixth bounce, it passes through the delay plane in the row above the blocks. The CC of mirror C′&D′ is located such that the beam goes from C′&D′ back to the delay plane, focusing to a spot on the flat segment of the segmented mirror (facing to the left). A close-up is shown in Fig. 9(b). This flat segment serves the same function as the flat mirror in the center of Fig. 8: It returns the light to C′&D′ and, from there, back through the delay plane (passing through the same row of the delay plane by which it entered) and back to the switching engine.

The light sent to the delay plane for the longest delay (bounce 8) will pass through the plane in the second row above the blocks. The light goes to C′&D′ as it did for the previous bit, but the image of the row now forms on a different segment of the segmented mirror: the bottom one. This segment is tilted to 7.5° to send the light to the other spherical mirror, labeled E&F. It has a dual name, because it is also an image of both C and D (images of these mirrors appear side by side on E&F). Mirror E&F reimages the spots from the bottom of the segmented mirror onto the top segment, which is tipped to 15° and directs the light back to E&F again. Then, the next spot appears on the opposite side of the CC (E&F), i.e., forms on the 7.5°-tipped segment again, and the light returns to C′&D′. From there, the

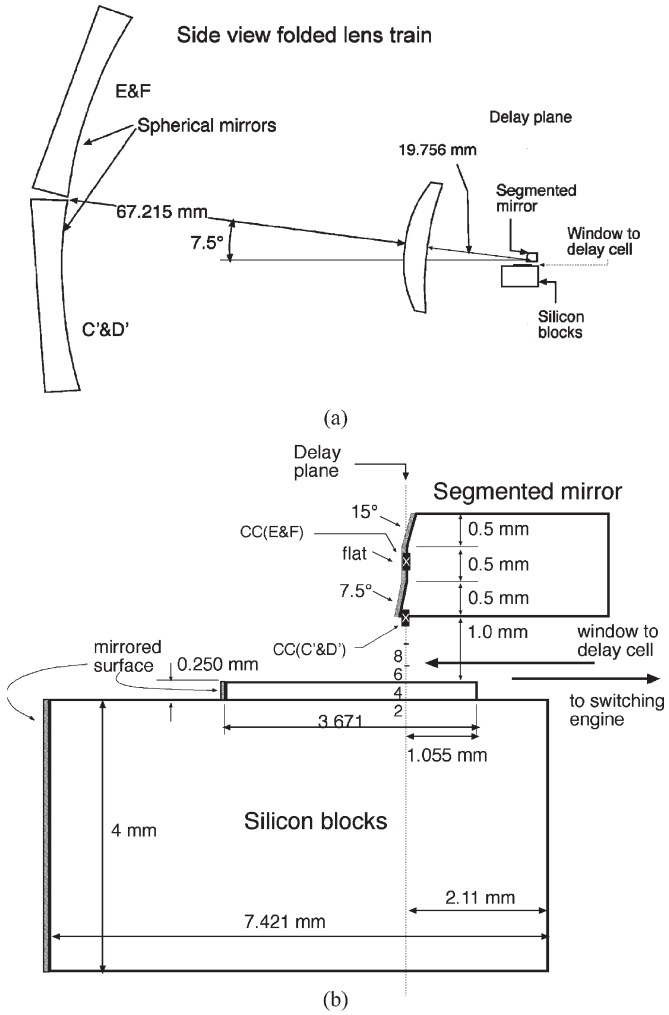

Fig. 9. (a) Folded lens train. (b) Close-up of delay plane.

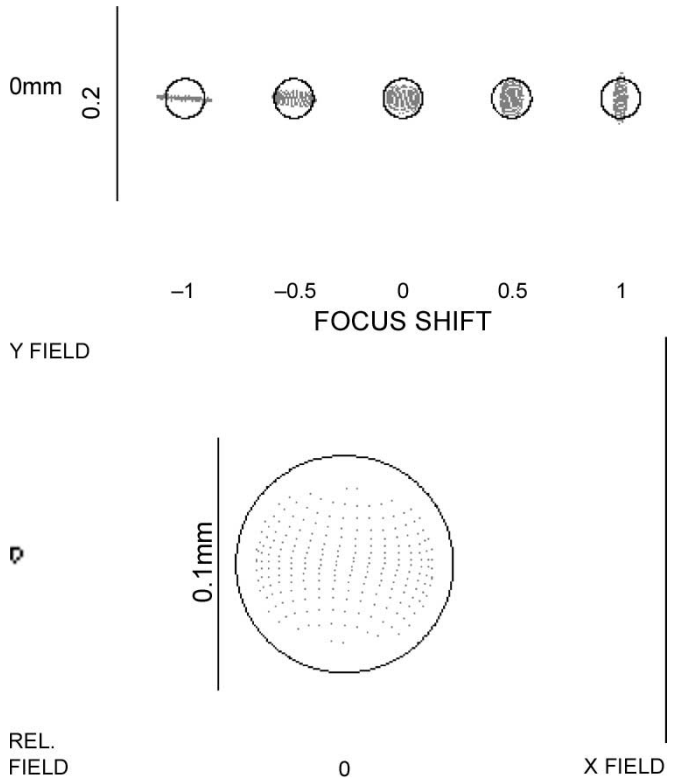

Fig. 10. Simulation results after 14 bounces in the switching engine, with a flat mirror in the delay plane. Some astigmatism is evident. However, even after 14 bounces, the spot is within the diffraction limit.

spots on the center segment are reimaged on the second row above the blocks of the delay plane again and return to the switching engine. Since the beam has effectively passed back and forth through the lens train twice as often as the previous bit, the delay is twice as long (2.5 ns).

2) Silicon Blocks: The two shortest delays ($\Delta = 78.125$ ps and $2\Delta = 156.25$ ps) are done in dielectric blocks. We choose optical-grade silicon because of its high refractive index (which shortens the block) and low absorption coefficient. The dimensions are shown in Fig. 9(b). The bottom block is made thick on purpose to provide mechanical support; light only travels through the top 0.25 mm. The blocks have antireflection coatings on the fronts (right side in the figure) and high-reflectivity coatings on the backs. The position of EACH block with respect to the delay plane is chosen to satisfy the two imaging conditions of White cells [5].

C. Simulation

The switching engine design of the 6-bit system was simulated in Optics Software for Layout and Optimization (OSLO). The MEMS/delay-plane combination is replaced with a flat mirror. We allow the beam to do all 14 bounces and send the beam to the delay arms each possible time (four times in all) and the other round trips are in the null cell. The 14th spot, which appears on the output turning mirror, is examined for evidence of aberration.

The image quality is shown in Fig. 10. The length of the vertical line at the left is 200 μm. There are five circles at the top of the figure, which represent the size of the diffraction-limited spot. A bundle of rays leaves the object, is reimaged by the White cell 14 times, and the spot pattern inside the circles show where the rays land at the last bounce. The center circle represents the place where the beam is focused, and point image spread patterns are shown for two positions before and after the focus. At the bottom of the figure is a close-up of the spot at focus. There is a small amount of astigmatism, but in all cases, the spots are well within the diffraction limit.

IV. Experiment

We built a proof-of-concept demonstration according to the design discussed in the previous section, using the unfolded lens train of Fig. 8. A custom assembly containing the silicon delay blocks and segmented mirror was not delivered in time to be demonstrated in this project.

To speed up alignment, we had a base plate made that had holes precisely located to accept rails, stages, and so on. Rails were also made, such that the field lens and White-cell mirror or each arm could be mutually aligned and the entire rail installed in the switching engine. To build the apparatus, we set up the optics for the switching engine on the rails, with the mirrors in

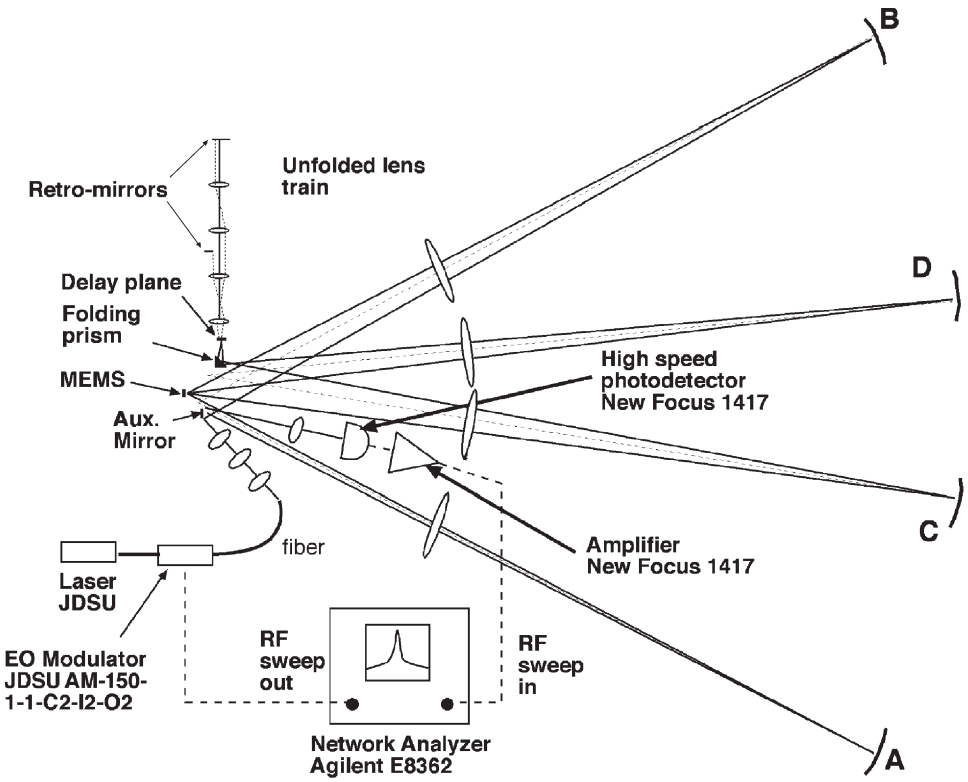

Fig. 11. Measurement setup for delays.

their nominal locations. We tweaked the focus and alignment as well as possible by eye, judging the spot size using a camera.

Then, we equalized the length of the null cell to the delay cell. We placed a flat mirror in the delay plane (no delay elements). We then measured the delay difference between the two paths using a network analyzer, as shown in Fig. 11. The RF sweep out (2–18 GHz) goes to a Mach–Zehnder modulator. The modulated output light goes through the time delay device and is detected by a high-speed photodetector. The electronic output is amplified and detected by the network analyzer, which performs a fast Fourier transform and displays the result. We calibrated the delay to the null cell (all nine bounces between A and B) and then sent the beam to C and D at every opportunity and measured the difference in time delay.

We found the path difference error to be 3.75 ps after initial alignment, which is surprisingly small. We then calculated the adjustments required in the longitudinal positions of C and D to equalize the times, taking into account that the flat mirror in the delay plane also had to be adjusted to maintain focus, and repeated the measurement. In two iterations, we adjusted C and D each longitudinally toward the MEMS by 381-μm total and moved the delay mirror away from the MEMS by 150 μm. The paths were now equalized to within the resolution of the measurement ($\pm$625 fs).

The spot pattern on the MEMS for the null cell is shown in Fig. 12(a) on the left. Here, we are using alternate rows of the MEMS. The MEMS is imaged (on the infrared camera) by shining a flashlight through the back of one of the White-cell mirrors (B). The dielectric mirrors, which are highly reflective at $\lambda = 1.55$ μm, will transmit visible light. The image of the MEMS is picked up by a pellicle placed in arm A. At the same time, infrared light is circulating through the White cell and creating spots on the MEMS. Note that the optics are focused for IR; the visible light reflecting from the MEMS pixels will necessarily be out of focus. We use this fuzzy image primarily to see which pixels the spots are on. However, the IR spots are in focus. On the right of the spot pattern is the network-analyzer output for the case when the beam is sent to the null cell on every pass. The horizontal axis is 2 ns/div and the vertical axis is 10 dB/div.

1) Delays: Then, the lens train was installed and aligned. We measured the delays for the first bit (1.25 ns), the second bit (2.5 ns), and both together (3.75 ns). Fig. 13(b)–(d) shows the spot pattern for each, along with the network-analyzer trace. The results shown were measured after the lens train was adjusted for the exact delays. Initially, after alignment by eye, the first bit of the lens train was off by 14 ps, and the second bit was off by 8 ps. In both cases, the adjustment is made by moving the retro-mirror until the delay is correct and then adjusting one of the lenses to reestablish focus. Once set, the delays were very stable.

Then, we explain the spot patterns. For the short delay (first bit), the light is sent to the delay cell on the second bounce on the MEMS. Recall that the pellicle that images the MEMS is in arm A. The IR beam is sent to the delay cell on the second bounce, so it does not go to arm A at all, which is why we cannot see that spot in Fig. 12(b). Also, the MEMS illumination is coming from arm B (recall the flashlight is held there), but the pixel is tipped, so the background light from that pixel also does not show up. On the third bounce on the MEMS, the beam is returned to the null cell, and the rest of the spots appear normally. The background light on the pixel does not appear on

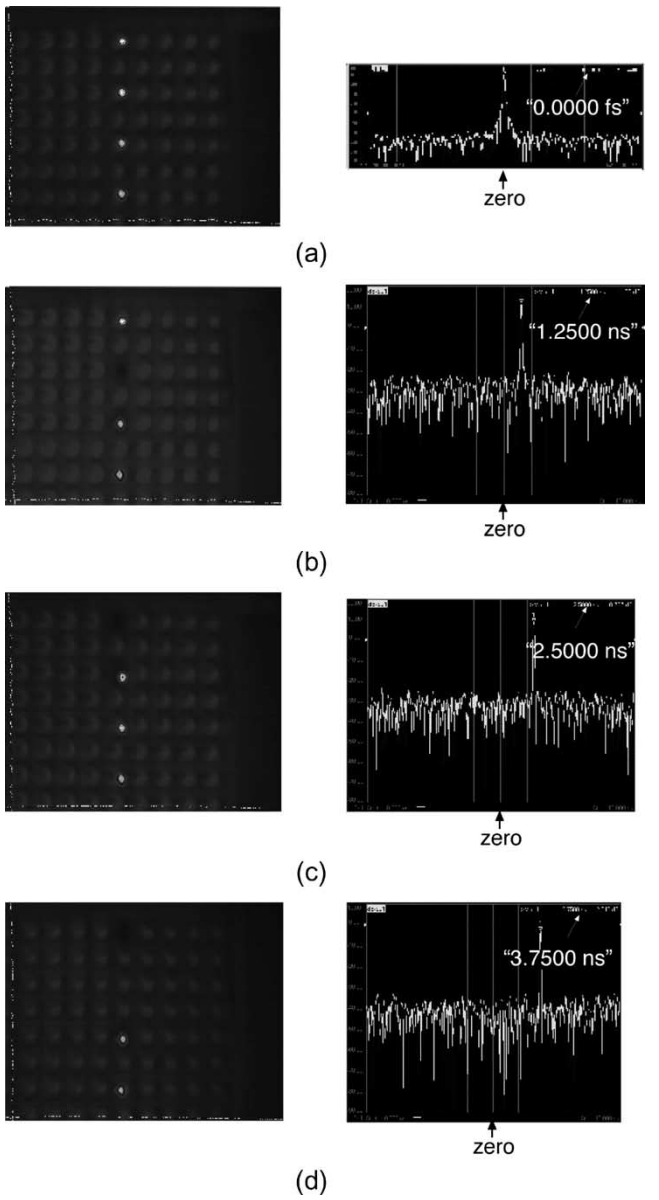

Fig. 12. Spot pattern on the MEMS (left) and time delays (right) for each of the four delays.

the third bounce because the pixel is tipped to bring the beam back into the null cell.

For the longer bit, the light is sent to the delay cell on the first bounce on the MEMS. The pixel is tipped also, so neither the IR spot nor the pixel appear. On the second bounce, the beam is sent back to the null cell, so the spot shows up. Again, the pixel is tipped, so the pixel lighting does not appear.

In the last photo, the first pixel is switched to send the beam to the delay cell. Neither the pixel nor the beam appears. On the second bounce, since we are visiting both delay bits, the pixel is flat, which keeps the beam in the delay cell for another round. Thus, the IR beam does not go to mirror A, but the backlight from B does appear in A; thus, we can see the second pixel.

2) Loss: We measured the loss in the binary White cell, for the null path and each of the delay paths, and did it for the case where the output went straight to a photodetector and for

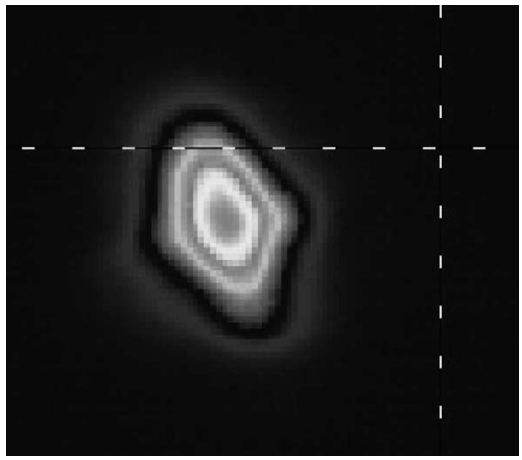

Fig. 13. Final spot after nine bounces in the White cell.

TABLE I
LOSS AS A FUNCTION OF PATH IN THE BINARY WHITE CELL

Path	Loss direct to detector	Loss including coupling into output fiber
All null cell	3.1 dB	10.3 dB
Short delay only	3.7 dB	11.7 dB
Long delay only	4.2 dB	11.3 dB
Both delays simultaneously	5.2 dB	14.0 dB

the case where the output was coupled back into fiber. There were nine total bounces, of which four were on the MEMS. We varied the number of times the beam was sent to the delay cell as opposed to the null cell. The results are shown in Table I. In the no-fiber case, the photodetector was a large-area detector so the quality and the size of the output spot should not have affected the results

We can explain at least some of the increase between the null cell and the short delay by recalling that, in the null path, the spot forms on a dielectric mirror (the auxiliary mirror); however, in the delay path, it encounters a gold-coated folding prism and two lenses and passes them twice: once over and once back. In addition, in our experiment, the retro-mirror at the end of the short delay was gold, not dielectric. For the longer delay, the prism is again encountered twice, and now, there are four lenses. However, in this case, the final mirror is dielectric. When both delays are visited, the beam passes the prism for a total of four times and passes through the first lenses four times, the second lenses twice, and strikes both the gold and the dielectric retro-mirrors.

Even accounting for all this, the losses are higher than one would like. In pursuing the cause, we measured the input beam and found that the spot was slightly larger than we designed for, i.e., it is possibly being clipped on each visit to the MEMS, and that the beam divergence was larger than expected, i.e., the beam was being truncated on each pass through the field lenses. The latter was verified by holding an IR-sensitive card to the edge of the field lenses and noting that there was in fact light there. The field lenses, which are 50.8 mm in diameter, are very close to the minimum diameter allowed by the beam divergence in the design. However, the White-cell mirrors could be smaller

but were chosen to be 50.8 mm for convenience (a standard diameter). Thus, there was truncation at the field lenses but not at the White-cell mirrors.

The truncation of the beams by the field lenses occurs only at the sides (not at the top and the bottom). This can be explained by returning to Fig. 5 and noting that the beam headed toward the White-cell mirror is not coincident with the returning beam but slightly offset sideways. The circular lens is just barely large enough to capture both beams side by side but more than tall enough. We therefore expect to see diffraction effects on the sides of the beam (but not the top and the bottom), and this is born out by the shape of the output spot, as shown in Fig. 13. The vertical elongation is the astigmatism mentioned in Section III. The rotation is due to the observation optics.

An output spot of this poor quality cannot be expected to couple well into fiber, and we see this effect in the last column of Table I, where the losses are worse by between 7 and almost 9 dB. The fiber is smaller than the large-area detector, so there is additional alignment sensitivity as well as distortion.

We next asked the following question: "How much does the MEMS contribute to the loss?" In particular, we were concerned that, if the MEMS micromirrors had any curvature, they would introduce extra diffraction. To assess this, we performed two experiments. We programmed the MEMS to have all mirrors flat, meaning the beam was confined to the null cell. We measured the loss. Then, we replaced the pixilated MEMS with a bulk gold mirror. The bulk mirror is assumed to be perfectly flat and definitely with no pixels, so no truncation can occur there.

With the MEMS in place, we found a total loss of 3.1 dB. On the other hand, we measured 2.9-dB loss with the plain gold mirror. Since the MEMS/gold mirror is visited four times, the worst contribution the MEMS can make to the overall loss is $0.2/4 = 0.05$ dB/bounce. Furthermore, if the MEMS were truncating or diffracting the beam or both, the effects would be expected to accumulate with successive bounces.

V. Physical Size

The experimental apparatus was intentionally made to be physically large to facilitate building and aligning on an optical table. In a real system, one would take care to choose optics as small as possible and then to use mirrors to fold the device into a compact volume. In a parallel study, we have shown that a 10-bit binary White cell, with delays from 9.78 to 10 ns, can be fit into a volume roughly $10 \times 10 \times 18$ cm $(4 \times 4 \times 7$ in). This particular design supports 532 antenna elements of a phased array radar (has 532 individual light beams circulating through it). The details will be published separately; here, we simply make the point that the White cell can be made very compact.

VI. Summary and Discussion

We have presented a design for a 6-bit OTTD device based on the White cell. The minimum delay is 78 ps, and the maximum delay is 5 ns. The design uses a 10×10-pixel MEMS micromirror array, with digital mirrors that can tip to one of three discrete positions. Light beams (one for each antenna element in the phased array) circulate in the White cell(s) and are refocused to spots once per round trip. The spots land on the MEMS pixels, and the MEMS is used to control which White cell the beam goes to on the next round trip: a null cell with no net delay or a White cell with delay elements. The delays are implemented as dielectric blocks for short delays and lens trains (that can be folded into more White cells) for long delays.

Experimentally, we demonstrated the operation of the binary White cell, switching between the White cells using MEMS, and the implementation of delays in an unfolded lens train. Delays could be easily established with the required accuracy (± 1.25 ps) while still fulfilling the multiple imaging conditions of White cells. The losses in the apparatus were between 3.1–5.2 dB when the output from the White cell was coupled directly to a photodetector; with output into the fiber, the loss was much worse. This was because of a problem with the input beam, of which the divergence was too large, causing truncation of the beam at the field lenses. This can be fixed with better input optics or larger field lenses.

The real strength of the White-cell approach is that many light beams, hundreds if necessary, can circulate simultaneously, and each can be individually controlled. In addition to the fact that all the light beams share the same hardware (mirrors, lenses, and delay lines), the White cell by its very nature is compact because the beams overlap constantly, which is one of the big benefits of using a free-space approach.

Acknowledgment

The authors would like to thank Prof. Em. S. A. Collins, Jr., for many helpful discussions and suggestions and O. B. Spahn and W. Cowan of Sandia National Laboratories for the MEMS, the MEMS drivers, and their help and support.

References

[1] B. L. Anderson and C. D. Liddle, "Optical true-time delay for phased array antennas: Demonstration of a quadratic White cell," *Appl. Opt.*, vol. 41, no. 23, pp. 4912–4921, Aug. 2002.

[2] B. L. Anderson and R. Mital, "Polynomial-based optical true-time delay devices using MEMs," *Appl. Opt.*, vol. 41, no. 26, pp. 5449–5461, Sep. 2002.

[3] S. A. Collins, Jr. and B. L. Anderson, *Device and Method for Producing Optically-Controlled Incremental Time Delays,* U.S. Patent 6 388 415, May 14, 2002.

[4] A. Rader and B. L. Anderson, "Demonstration of a linear optical true-time delay device using a microelectromechanical mirror array," *Appl. Opt.*, vol. 42, no. 8, pp. 1409–1416, Mar. 2003.

[5] S. Kunathikom, B. L. Anderson, and S. A. Collins, Jr., "Design of delay elements in binary optical true-time delay device using a White cell," *Appl. Opt.*, vol. 42, no. 35, pp. 6984–6994, Dec. 2003.

[6] R. Higgins, N. K. Nahar, and B. L. Anderson, "Design and demonstration of a switching engine for a binary true-time delay device using a White cell," *Appl. Opt.*, vol. 42, no. 23, pp. 4657–4747, Aug. 2003.

[7] J. White, "Long optical paths of large aperture," *J. Opt. Soc. Amer.*, vol. 32, no. 5, pp. 285–288, May 1942.

[8] B. L. Anderson, V. Argueta-Diaz, F. Abou-Galala, G. Radhakrishnan, and R. Higgins, "Optical cross-connect switch based on tip/tilt micromirrors in a White cell," *IEEE J. Sel. Topics Quantum Electron.*, vol. 9, no. 2, pp. 579–593, Mar./Apr. 2003.

Betty Lise Anderson (S'75–M'79–SM'95) received the B.S. degree in electrical engineering from Syracuse University, Syracuse, NY, and the M.S. and Ph.D. degrees in materials science and electrical engineering from the University of Vermont, Burlington, in 1978, 1988, and 1990, respectively.

She spent nine years in industrial companies including Tektronix, Inc., GTE Laboratories, and Draper Laboratories. She is currently a Professor at the Department of Electrical and Computer Engineering, The Ohio State University, Columbus. Her current research interests include analog optical signal processing, devices for optical communication systems, coherence, and semiconductor devices. She is the coauthor (with R. L. Anderson) of *Fundamentals of Semiconductor Devices* (Burr Ridge, IL: McGraw-Hill, 2005).

Prof. Anderson is a member of the Optical Society of America. She is an Associate Editor for IEEE JOURNAL OF QUANTUM ELECTRONICS.

David J. Rabb was born in Columbus, OH, on June 15, 1979. He received the B.S. degree from Ohio University, Athens, and the M.S. degree specializing in optics from The Ohio State University, Columbus, in June 2002 and December 2005, respectively, both in electrical engineering.

Since January 2003, he has worked as a Research Assistant at the ElectroScience Laboratory at The Ohio State University. In 2005, he was a summer Intern at Sandia National Laboratories, Sandia, NM.

Carolyn M. Warnky received the B.S. degree in electronic engineering from Southern Illinois University-Edwardsville, and the M.S. and Ph.D. degrees in electrical engineering from The Ohio State University, Columbus, in 1979, 1994, and 2002, respectively.

She was a Post-Doctoral Researcher at The Ohio State University at the time of this research.

Dr. Warnky is a member of the Optical Society of America.

Feras Abou-Galala (S'00) received the B.S. degree from the University of Qatar, Doha, Qatar, and the M.S. degree from The Ohio State University, Columbus, in 2000 and 2003, respectively, both in electrical engineering. He is currently working toward the Ph.D. degree at the Electrical Engineering Department (photonics and optics), The Ohio State University.

His current research interests include all-optical networking devices, QoS in optical communication networks, and optical signal processing.

Mr. Abou-Galala is a member of the Society of Photo-Optical Instrumentation Engineers.